

# Evaluation of Spatial Distortion in Multichannel Audio

Karn N. Watcharasupat, *Graduate Student Member, IEEE*, and Alexander Lerch, *Member, IEEE*

**Abstract**—Despite the recent proliferation of spatial audio technologies, the evaluation of spatial quality continues to rely on subjective listening tests, often requiring expert listeners. Based on the duplex theory of spatial hearing, it is possible to construct a signal model for frequency-independent spatial distortion by accounting for inter-channel time and level differences relative to a reference signal. By using a combination of least-square optimization and heuristics, we propose a signal decomposition method to isolate the spatial error from a processed signal. This allows the computation of simple energy-ratio metrics, providing objective measures of spatial and non-spatial signal qualities, with minimal assumption and no dataset dependency. Experiments demonstrate robustness of the method against common signal degradation as introduced by, e.g., audio compression and music source separation.

**Index Terms**—Multichannel signal processing, signal decomposition, spatial audio, quality evaluation

## I. INTRODUCTION

THE development of spatial audio technology is intrinsically linked to the spatial hearing ability of human listeners. Human sound localization is commonly understood to be characterizable by the head-related transfer function (HRTF), whereby the shapes and locations of the head, ears, and other anatomical features transform how the sound source originating from a particular location is finally received by the ear. A simplified understanding of this phenomenon, known as the duplex theory [1], can be thought of in terms of the frequency-independent interaural time differences of arrival and the interaural level differences of sound sources between the ears.

The duplex theory, in particular, has been exploited to achieve significant data compression in various lossy audio codec, such as MP3 [2], AAC [3], Vorbis [4], and Opus [5]. These techniques, however, are known to produce audible spatial artifacts, especially at lower bitrates [6, 7]. Although spatial artifacts resulting from such encoding have been repeatedly shown to affect overall perception of audio quality [8–10], to the best of our knowledge, few experimental studies have specifically investigated objective measurements of these spatial artifacts. Unsurprisingly, equally few objective metrics have been designed specifically for spatial evaluation of multichannel audio. Most practical evaluation of spatial quality continues to rely on time-consuming and labor-intensive listening tests, often requiring expert listeners [11]. A number of spectral and spatial features were proposed for training a simple model to predict

perceptual ratings [12–15]. More recently, a similar deep neural metric was proposed in [16] for binaural audio. All of these data-dependent approaches, however, are not usable outside the channel configuration in which the prediction models were trained on. The generalizability of the models are also often called into question when applying the predictor to unseen data with significant domain shift. AMBIQUAL, a metric designed for ambisonic signals derived from structural similarities of the time-frequency representations [17, 18], does not suffer from data dependency but was designed only for ambisonic data.

Despite limited literature specific to spatial evaluation, findings from audio quality evaluation in other subdomains can be adapted for spatial audio evaluation. In multichannel blind source separation (BSS), the `bsseval` toolbox [19–21] has been used widely to measure various aspects of signal degradation due to BSS algorithms. To account for filtering error, the toolbox computes a 512-tap least-square multichannel projection filter  $\mathbf{h}$  of reference signal  $\mathbf{s}$  onto the estimated signal  $\hat{\mathbf{s}}$ . However, among other criticisms [22], the resulting error signal  $\mathbf{e}_{\text{proj}} = \mathbf{s} * \mathbf{h} - \hat{\mathbf{s}}$  has often been referred to as the “spatial error” signal, despite containing all filtering errors accountable within 512 taps regardless of their spatial relevance. This issue in particular has led to the limited utility of the “source image to spatial distortion ratio” (ISR), relative to other metrics in the widely used `bsseval` toolbox.

By constraining the projection filter, however, it is possible to exclusively account for some spatial distortion, in particular those accounted for by the duplex theory, due to their frequency independence. Spatial information originating from the room acoustics or head-related transfer functions, however, cannot be easily distinguished *a priori* from other frequency-dependent distortion. In this work, we propose a decomposition technique<sup>1</sup> that distinguishes a subset of spatial distortion from other filtering distortion, allowing the energy ratio between a clean signal and the corresponding spatial error signal to be explicitly computed. The technique was designed such that it can be used either independently for, e.g., codec evaluation, or in conjunction with existing ratio metrics for evaluation of source separation systems.

## II. PROPOSED METHOD

### A. Signal Model and Spatial Projection

In a multichannel audio setting, the filtering error itself can be loosely decomposed into one concerning spatial distortion, such as interchannel time differences (ITD) and interchannel level

Both authors are with the Music Informatics Group, Georgia Institute of Technology, Atlanta, GA 30332 USA (email: kwatcharasupat@gatech.edu; alexander.lerch@gatech.edu).

<sup>1</sup>Implementation is available at [github.com/karnwatcharasupat/spauq](https://github.com/karnwatcharasupat/spauq). Last accessed: June 16, 2023.

differences (ILD), and another concerning frequency response distortion, such as changes in equalization (EQ) or timbre. Admittedly, any spatial effect with a frequency-dependent response, such as the those due to room reverberation or the pinna filtering effects, cannot be fully distinguished from EQ distortion. As such, we will only consider filtering operations related to the duplex theory in this work.

Changes to the ITD can be modeled by relative changes in delays over the channels, while changes to the ILD can be modeled by relative changes in the gain of each channel as well as leakages into other channels. For a signal  $\mathbf{s}$  with  $C$  channels, the projected signal  $\tilde{\mathbf{s}}$  can thus be modeled by

$$\tilde{s}_c[n] = \sum_d A_{cd} s_d[n - \tau_{cd}], \quad \forall c, n. \quad (1)$$

Since we are interested in projecting the *reference* signal as close to the *estimated* signal as possible, this results in the least-square optimization objective  $\min_{\mathbf{A}, \mathbf{T}} \|\tilde{\mathbf{s}} - \hat{\mathbf{s}}\|^2$  where  $(\mathbf{T})_{cd} = \tau_{cd}$ .

At an optimal  $\mathbf{T}$ , the optimal value for each row of  $\mathbf{A}$  can be found by solving the matrix equation<sup>2</sup>

$$\mathbf{A}_{c,:} \mathbf{R}^c = \hat{\mathbf{R}}_{c,:}, \quad (2)$$

$$(\mathbf{R}^c)_{bd} = \sum_n s_b[n - \tau_{cb}] s_d[n - \tau_{cd}], \quad (3)$$

$$(\hat{\mathbf{R}})_{cd} = \sum_n \hat{s}_c[n] s_d[n - \tau_{cd}]. \quad (4)$$

Solving for  $\mathbf{T}$  directly remains an open problem due to multiple local minima and non-monotonic gradients. As such, we used a method based on interchannel correlation to assign

$$\tau_{cd} = \arg \max_{\eta} \left| \sum_n \hat{s}_c[n] s_d[n - \eta] \right|. \quad (5)$$

In other words, each input channel of the reference signal is shifted so that it is maximally correlated to target channel of the estimate signal or its inversion.

### B. Energy-Ratio Metrics

Once the optimal projection  $\tilde{\mathbf{s}}$  is found, the spatial error signal can be computed using  $\mathbf{e}_{\text{spat}} = \tilde{\mathbf{s}} - \mathbf{s}$ , while any other residual error can be computed by treating  $\tilde{\mathbf{s}}$  as the ‘new’ reference, i.e.,  $\mathbf{e}_{\text{resid}} = \hat{\mathbf{s}} - \tilde{\mathbf{s}}$ . Thus, the total error between the reference and the estimated signal can be written as

$$\mathbf{e}_{\text{total}} = \hat{\mathbf{s}} - \mathbf{s} = \mathbf{e}_{\text{spat}} + \mathbf{e}_{\text{resid}}. \quad (6)$$

Using the decompositions above, two metrics naturally arise, namely the Signal to Spatial Distortion Ratio (SSR),

$$\text{SSR}(\hat{\mathbf{s}}; \mathbf{s}) = 10 \log_{10} \frac{\|\mathbf{s}\|^2}{\|\mathbf{e}_{\text{spat}}\|^2}, \quad (7)$$

and the Signal to Residual Distortion Ratio (SRR),

$$\text{SRR}(\hat{\mathbf{s}}; \mathbf{s}) = 10 \log_{10} \frac{\|\tilde{\mathbf{s}}\|^2}{\|\mathbf{e}_{\text{resid}}\|^2}. \quad (8)$$

The SSR itself can be considered as a replacement of the ISR, considering only components of the error signals with

spatial importance as errors. The SRR effectively acts as the non-spatial SNR, only considering non-spatial errors such as interference, timbral distortion, and additive artifacts.

### C. Framewise Computation

Since the proposed decomposition is relatively easy to compute, the computation can be made in a frame-wise manner. This is particularly helpful in the case of time-variant signals such as music, speech, and environmental sound where the signal content can drastically change over a time period. This means that most audio processing algorithms may also process the signal in a time-variant manner, leading to time-varying spatial distortion which in turns requires time-varying decomposition. Following `bsseval`, we defaulted to a window of 2s with 50% overlap in our implementation.

## III. SIGNAL DEGRADATION TESTS

To evaluate the robustness of the proposed decomposition and thus the proposed metrics, common signal degradations and spatial distortions are evaluated on a subset of the TIMIT Acoustic-Phonetic Continuous Speech Corpus [23]. For the purpose of this robustness check we test various audio degradation on recorded utterances of the sentence SA1, as uttered by 168 different participants with various dialectical variants of American English; SA1 is chosen as it was designed to expose diverse variations in English phoneme pronunciation. The TIMIT Corpus provides single-channel 16-bit PCM audio signal sampled at 16 kHz. In order to simulate known spatialization settings, each mono signal is spatialized to a stereo setup using the constant-power pan law

$$g_L = \cos\left(\frac{\pi}{4}(p+1)\right), \quad g_R = \sin\left(\frac{\pi}{4}(p+1)\right) \quad (9)$$

with  $p \in [-1, 1]$ .

### A. Panning Error

The most basic test is to investigate the relationship between the metrics in the case where there is only spatial error and no other type of degradation. This first test is simulated by considering magnitude-only stereo panning errors between the estimate signals and the reference signals. For the stereo setup defined in Eq. (9), the theoretical SRR is positive infinity while the theoretical SSR is given by<sup>2</sup>

$$-10 \log_{10} \left[ 2 - 2 \cos\left(\frac{\pi}{4}(\hat{p} - p)\right) \right], \quad (10)$$

where  $p$  is the pan parameter of the reference signal and  $\hat{p}$  is the pan parameter of the signal estimate.

As theoretically expected, all computed SRR values on the SA1 signals of the TIMIT Corpus test set were all effectively positive infinities and are not plotted here due to space constraints. The SSR results are shown in Figure 1 and are consistent with the theoretical values with very small variances.

<sup>2</sup>See Supplementary Materials for derivation.

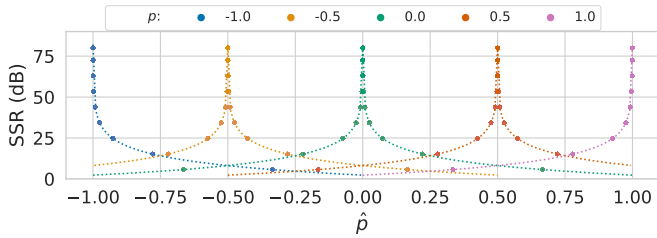


Fig. 1. SSR of the estimate signals with respect to the pan parameters. Circular markers represent the experimental values. Dotted lines represent the theoretical values.

### B. Delay Error

The next test is concerning the channel-wise delay error. The reference signal for this experiment is center-panned ( $p = 0$ ) with no delay applied. The estimate signals are panned at various errors, with an additional delay of  $\hat{d}_R$  samples applied only on the right channel. In this setup, the theoretical value of the SRR is positive infinity while that of the SSR is given by<sup>2</sup>

$$-10 \log_{10} \left[ 2 - 2 \cos \left( \frac{\pi \hat{p}}{4} \right) + 2g_R \hat{g}_R \left( 1 - \frac{\kappa[\hat{d}_R]}{\kappa[0]} \right) \right] \quad (11)$$

where  $\kappa[\cdot]$  is the autocorrelation function of the mono signal.

The results of the delay test are shown in Figure 2. In general, most experimental values lie within or close to the expected range. Within each pan parameter, the SSR follows roughly the shape of the autocorrelation function of a speech signal with minima roughly at the delay where the shifted speech signal would be at maximally negative correlation with the unshifted version of itself. With the exception of  $\hat{p} = -1$ , where only the left channel of the estimate is present, the distributions of the SRR are nearly identical across all pan values. At lower delays, more SRR values are at concentrated the expected positive infinity (capped at 80 dB for numerical stability). As the delays increases, the SRR values tend to decrease, but remain at relatively high values above 25 dB. Upon inspection of the decomposition, the channel-wise shift values have been estimated correctly for all test signals while the channel-wise gain values are often only *approximating* the ideal values, with the deviation increasing with  $\hat{d}_R$ . The slightly imperfect projection thus results in the observed spread and deviation in the SRR values from the theoretical values.

### C. Filtering Error

Many audio processing algorithms can cause a loss of bandwidth [6, 24]. To test the ability of the proposed method to distinguish other filtering errors from spatially relevant ones, the estimates were forward-backward filtered with a 128-tap low pass filter computed using the Remez exchange algorithm at various cutoff frequencies  $f_c$  with a transition band of one third-octave. The reference signal for this experiment is center-panned ( $p = 0$ ) with no delay applied. The theoretical SSR for this test is given in Eq. (10).

The results of this test are shown in Figure 3. As expected, the SRR increases monotonically as the cutoff frequency increases. At high cutoff frequencies, the SSR is close to

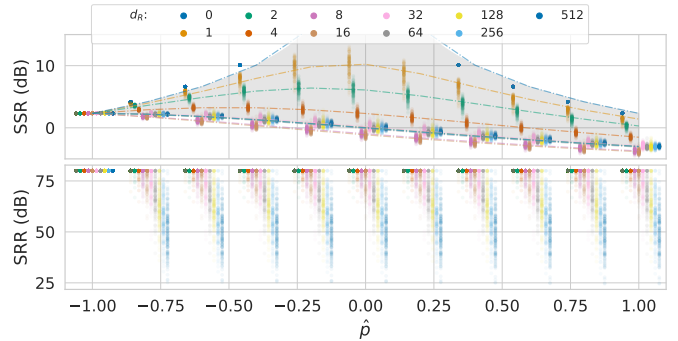


Fig. 2. SSR (top) and SRR (bottom) of the estimate signals with respect to the pan and right-channel delay parameters. Circular markers represent the experimental values with the horizontal axis slightly offset for readability. In the top plot, the dashdotted lines connect the median value of the SSR for each delay value; the gray area represents the theoretical range of the SSR.

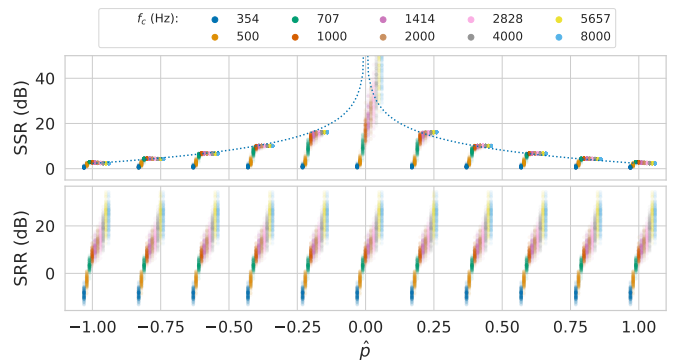


Fig. 3. SSR (top) and SRR (bottom) of the estimate signals with respect to the cutoff frequencies and pan parameters. Circular markers represent the experimental values with the horizontal axis slightly offset for readability. In the top plot, the dotted lines represent the theoretical values of the SSR.

the theoretical value. As more of the signal content is lost with decreasing cutoff frequency, the SSR also decreases, with large deviation below 1 kHz. This is somewhat expected given that spatial decomposition will only be valid if most of the signal content is present.

### D. Additive Noise

Another common audio degradation is the addition of noise or other uncorrelated artifacts. In the presence of an uncorrelated additive noise, the SRR is theoretically the overall SNR itself, while the theoretical SSR is given by Eq. (10), independent of the SNR. The computed metrics after adding random Gaussian noise at various SNRs are shown in Figure 4. At  $\hat{p} \neq 0$ , where the theoretical values are finite, the SSR generally follows the theoretical values with small spread except for the most noisy case where the SNR is  $-24$  dB, demonstrating that the decomposition is generally robust to noise. The experimental SRR values largely follow the SNRs themselves with small spreads, demonstrating that the residual errors consist almost entirely of non-spatial errors.

## IV. BENCHMARKS

As a benchmark for the newly introduced metrics, we apply audio compression and music source separation algorithms on the MUSDB18-HQ dataset [25], which provide

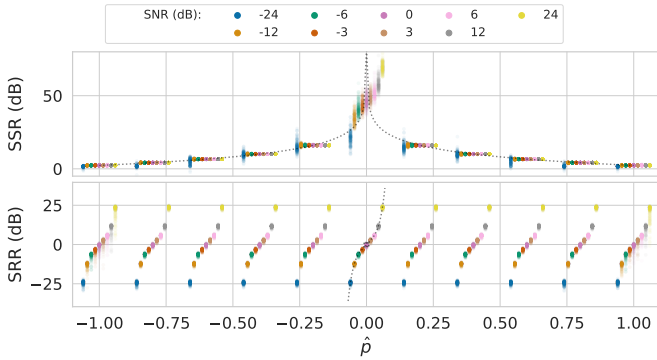


Fig. 4. SSR (top) and SRR (bottom) of the estimate signals with respect to the pan and SNR parameters. Circular markers represent the experimental values with the horizontal axis slightly offset for readability. The dotted lines represent the theoretical values.

50 uncompressed stereo music signals sampled at 44.1 kHz. Audio compression and music source separation are specifically chosen as test cases as these are known to introduce both spatial and non-spatial artifacts on music signals.

#### A. Codec

As a benchmark, we apply AAC (FAAC 1.30; FAAD2 2.10.0-2), and Opus (libopus 1.3.1) to the test set of MUSDB18-HQ to investigate their impact on SSR and SRR at bitrates from 32 to 320 Kbps. For AAC, the changes in SSR and SRR at each bitrate compared to no joint encoding are shown in Figure 5. Additional plots are provided in the Supplementary Materials. For both AAC and Opus, both SSR and SRR increase as the bitrate increases. The trend in SSR is consistent with the literature on Opus [26, 27] where localization errors increase with decreasing bitrate. In AAC, both mid/side stereo (MS) and intensity stereo (IS) modes generally performed worse in SSR than no joint coding across most ABRs, except for the MS mode at very low ABRs of 32 Kbps and 40 Kbps. In particular, IS also consistently performed worse than MS up to an ABR of 192 Kbps. This is consistent with the knowledge that IS can cause severe spatial artifacts, especially for low-frequency content with decorrelated spatial images [6, 7, 28]. In terms of SRR, which effectively measures the non-spatial fidelity of the codec, the MS mode performs better than no joint coding up to about 112 Kbps while intensity stereo only performs better than no joint coding below 64 Kbps. It is expected that no joint coding performs better than joint coding from about 128 Kbps onwards since joint coding can introduce unnecessary information loss at these bitrates [7].

#### B. Music Source Separation

To benchmark the proposed metrics on the music source separation task, we apply Hybrid Demucs (v3) [29], ConvTasNet [30], OpenUnmix [31], and Spleeter [32] on the test set of MUSDB18-HQ. OpenUnmix and Spleeter perform separation in the time-frequency domain using real-valued channel-wise masks on the complex-valued short-time Fourier transform (STFT) spectrogram. ConvTasNet similarly performs real-valued mask-based separation but on a learnable real-valued basis transform. Hybrid Demucs is the only model

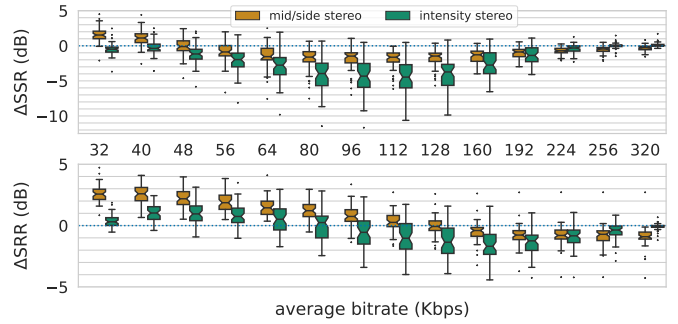


Fig. 5. Change in SSR and SRR of the test signals compressed by AAC, relative to the operating mode without joint encoding, by operating mode and average bitrates.

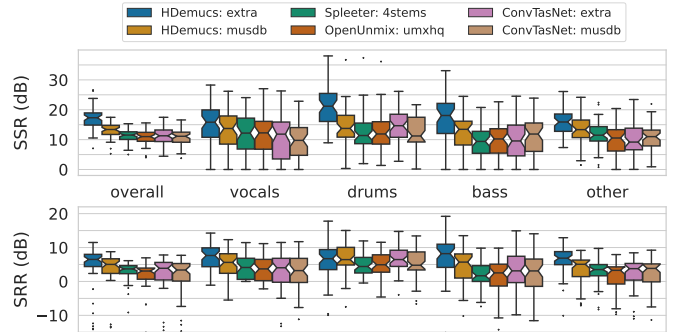


Fig. 6. Evaluation results on the MUSDB18-HQ test set.

tested here that does not utilize masking, instead modifying the time-domain signal and the STFT representation directly in its time and time-frequency branches, respectively. Note that OpenUnmix and Spleeter were optimized in the time-frequency domain without considering phase information, while ConvTasNet and Hybrid Demucs were optimized in the time domain.

The performance of the models is shown in Figure 6. The suffix behind the model name refers to the pre-trained weight variants provided by the model developers<sup>3</sup>. The SRR values, which effectively act as a non-spatial counterpart of the SDRs, are consistent with the SDRs reported in literature. In terms of SSR, Demucs performs the best among the tested models, while other models perform approximately on par with one another. We surmise that the superior performance of Demucs may be due to either or a combination of (i) its non-masking nature, (ii) the use of a direct time-domain processing branch, and/or (iii) direct optimization in the time domain.

#### V. CONCLUSION

In this work, we proposed a spatial evaluation method using filter decomposition technique based on the Duplex theory of spatial hearing. Tests on common signal degradation demonstrated relatively robust performance. The proposed method is additionally benchmarked on audio compression algorithms and music source separation algorithms, showing results consistent with perceptual literature. An open-source Python implementation of the proposed method is provided.

<sup>3</sup>The training data of HDemucs:extra also contains the test set of MUSDB18-HQ thus may not provide a fair comparison to the rest of the models which has not seen the test set in its training data.

## REFERENCES

- [1] L. Rayleigh, "On our perception of sound direction," *London, Edinburgh, Dublin Philos. Mag. J. Sci.*, vol. 13, no. 74, pp. 214–232, 1907.
- [2] International Organization for Standardization, "ISO/IEC 13818-3:1998 Information technology — Generic coding of moving pictures and associated audio information — Part 3: Audio," 1998.
- [3] —, "ISO/IEC 13818-7:2006 Information technology — Generic coding of moving pictures and associated audio information — Part 7: Advanced Audio Coding (AAC)," 2006.
- [4] Xiph.Org Foundation, "Vorbis I specification," Tech. Rep., 2020.
- [5] J.-M. Valin, K. Vos, and T. Terriberry, "RFC 6716: Definition of the Opus audio codec," 2012.
- [6] K. Brandenburg, "MP3 and AAC explained," in *Proc. 17th AES Int. Conf. High-Quality Audio Coding*, 1999.
- [7] J. Herre, "From Joint Stereo to Spatial Audio Coding - Recent Progress and Standardization," in *Proc. 7th Int. Conf. Digit. Audio Eff.*, 2004, pp. 157–162.
- [8] F. Rumsey, S. Zielinski, R. Kassier, and S. Bech, "On the relative importance of spatial and timbral fidelities in judgments of degraded multichannel audio quality," *J. Acoust. Soc. Am.*, vol. 118, no. 2, pp. 968–976, 2005.
- [9] P. M. Delgado and J. Herre, "Objective Assessment of Spatial Audio Quality Using Directional Loudness Maps," in *Proc. IEEE Int. Conf. Acoust. Speech Signal Process.*, 2019, pp. 621–625.
- [10] —, "Investigations on the Influence of Combined Inter-Aural Cue Distortions in Overall Audio Quality," in *Proc. Deutsche Jahrestagung für Akustik*, 2019, pp. 907–910.
- [11] A. Lindau, V. Erbes, S. Lepa, H.-J. Maempel, F. Brinkman, S. Weinzierl, A. Lindau, V. Erbes, S. Lepa, H.-J. Maempel, and F. Brinkman, "A Spatial Audio Quality Inventory (SAQI)," *Acta Acustica united with Acustica*, vol. 100, no. 5, pp. 984–994, 2014.
- [12] S. George, S. Zielinski, and F. Rumsey, "Feature Extraction for the Prediction of Multichannel Spatial Audio Fidelity," *IEEE Trans. Audio, Speech, Lang. Process.*, vol. 14, no. 6, pp. 1994–2005, 2006.
- [13] —, "Initial developments of an objective method for the prediction of basic audio quality for surround audio recordings," in *Proc. 120th AES Conv.*, 2006.
- [14] I. Choi, S. B. Chon, B. G. Shinn-Cunningham, and K. Sung, "Prediction of Perceived Quality in Multi-Channel Audio Compression Coding Systems," in *Proc. AES 30th Int. Conf. Intell. Audio Environ.*, 2007.
- [15] I. Choi, B. G. Shinn-Cunningham, S. B. Chon, and K.-M. Sung, "Objective measurement of perceived auditory quality in multichannel audio compression coding systems," *J. Audio Eng. Soc.*, vol. 56, no. 1/2, pp. 3–17, 2008.
- [16] P. Manocha, A. Kumar, B. Xu, A. Menon, I. D. Gebru, V. K. Ithapu, and P. Calamia, "SAQAM: Spatial Audio Quality Assessment Metric," in *Proc. Annu. Conf. Int. Speech Commun. Assoc.*, 2022, pp. 649–653.
- [17] M. Narbutt, A. Allen, J. Skoglund, M. Chinen, and A. Hines, "AMBIQUAL - a full reference objective quality metric for ambisonic spatial audio," in *Proc. 10th Int. Conf. Qual. Multimed. Exp.*, 2018, pp. 1–6.
- [18] M. Narbutt, J. Skoglund, A. Allen, M. Chinen, D. Barry, and A. Hines, "AMBIQUAL: Towards a Quality Metric for Headphone Rendered Compressed Ambisonic Spatial Audio," *Appl. Sci.*, vol. 10, no. 9, 2020.
- [19] E. Vincent, R. Gribonval, and C. Févotte, "Performance measurement in blind audio source separation," *IEEE Trans. Audio Speech Lang. Process.*, vol. 14, no. 4, pp. 1462–1469, 2006.
- [20] E. Vincent, H. Sawada, P. Bofill, S. Makino, and J. P. Rosca, "First stereo audio source separation evaluation campaign: Data, algorithms and results," in *Proc. Int. Conf. Indep. Compon. Analysis Signal Sep.*, 2007, pp. 552–559.
- [21] E. Vincent, S. Araki, F. Theis, G. Nolte, P. Bofill, H. Sawada, A. Ozerov, V. Gowreesunker, D. Lutter, and N. Q. Duong, "The Signal Separation Evaluation Campaign (2007-2010): Achievements and Remaining Challenges," *Signal Process.*, vol. 92, no. 8, pp. 1928–1936, 2012.
- [22] J. Le Roux, S. Wisdom, H. Erdogan, and J. R. Hershey, "SDR - Half-baked or Well Done?" in *Proc. IEEE Int. Conf. Acoust. Speech Signal Process.*, 2019, pp. 626–630.
- [23] J. S. Garofolo, L. F. Lamel, W. M. Fisher, J. G. Fiscus, D. S. Pallett, N. L. Dahlgren, and V. Zue, "TIMIT Acoustic Phonetic Continuous Speech Corpus," 1993.
- [24] N. Schaffer, B. Cogan, E. Manilow, M. Morrison, P. Seetharaman, and B. Pardo, "Music Separation Enhancement with Generative Modeling," in *Proc. 23rd Int. Soc. for Music. Inf. Retr. Conf.*, 2022, pp. 772–780.
- [25] Z. Rafii, A. Liutkus, F.-R. Stöter, S. I. Mimitakis, and R. Bittner, "The MUSDB18 corpus for music separation," 2017.
- [26] M. Narbutt, S. O'Leary, A. Allen, J. Skoglund, and A. Hines, "Streaming VR for immersion: Quality aspects of compressed spatial audio," in *Proc. 23rd Int. Conf. Virtual Syst. & Multimed.*, 2017, pp. 1–6.
- [27] T. Rudzki, I. Gomez-Lanzaco, J. Stubbs, J. Skoglund, D. T. Murphy, and G. Kearney, "Auditory localization in low-bitrate compressed Ambisonic scenes," *Appl. Sci. (Switzerland)*, vol. 9, no. 13, 2019.
- [28] J. Herre, K. Brandenburg, and D. Lederer, "Intensity stereo coding," in *Audio Eng. Soc. Conv. 96*, 1994.
- [29] A. Défossez, "Hybrid Spectrogram and Waveform Source Separation," in *Proc. Music. Demixing Workshop*, 2021.
- [30] Y. Luo and N. Mesgarani, "Conv-TasNet: Surpassing Ideal Time-Frequency Magnitude Masking for Speech Separation," *IEEE/ACM Trans. Audio Speech Lang. Process.*, vol. 27, no. 8, pp. 1256–1266, 2019.
- [31] F.-R. Stöter, S. Uhlich, A. Liutkus, and Y. Mitsufuji, "Open-Unmix - A Reference Implementation for Music Source Separation," *J. Open Source Softw.*, vol. 4, no. 41, p. 1667, 2019.
- [32] R. Hennequin, A. Khlif, F. Voituret, and M. Moussallam, "Spleeter: a fast and efficient music source separation tool with pre-trained models," *J. Open Source Softw.*, vol. 5, no. 50, p. 2154, 2020.

## Supplementary: Evaluation of Spatial Distortion in Multichannel Audio

Karn N. Watcharasupat, *Graduate Student Member, IEEE*, and Alexander Lerch, *Member, IEEE*

### A. DERIVATION OF THE OPTIMAL GAIN MATRIX

Denote the objective function to be minimized by

$$\mathcal{L}(\mathbf{A}, \mathbf{T}) = \sum_n \|\tilde{\mathbf{s}}[n] - \hat{\mathbf{s}}[n]\|^2 \quad (\text{A.1})$$

$$= \sum_n (\tilde{\mathbf{s}}^T[n]\tilde{\mathbf{s}}[n] - 2\tilde{\mathbf{s}}^T[n]\hat{\mathbf{s}}[n] + \hat{\mathbf{s}}^T[n]\hat{\mathbf{s}}[n]). \quad (\text{A.2})$$

Taking the derivative with respect to  $\mathbf{A}$  gives

$$\frac{\partial \mathcal{L}}{\partial A_{ij}} = 2 \sum_n (\tilde{s}_i[n] - \hat{s}_i[n])s_j[n - \tau_{ij}], \quad (\text{A.3})$$

since

$$\frac{\partial \tilde{s}_c[n]}{\partial A_{ij}} = \mathbb{I}[i = c]s_j[n - \tau_{ij}], \quad (\text{A.4})$$

where  $\mathbb{I}[\cdot]$  is the Iverson bracket. By setting the derivative to zero, we have

$$\sum_n \hat{s}_i[n]s_j[n - \tau_{ij}] = \sum_n \tilde{s}_i[n]s_j[n - \tau_{ij}] \quad (\text{A.5})$$

$$= \sum_d A_{id} \sum_n s_d[n - \tau_{id}]s_j[n - \tau_{ij}] \quad (\text{A.6})$$

which reduces to (3).

### B. DERIVATION OF THE THEORETICAL SSR

For this section, let  $\text{SSR} = 10 \log_{10} u$ . Denote the mono reference signal by  $v$ . Let  $E_v = \sum_n v^2[n]$ . Considering only the necessary parametrization for III.A and III.B,

$$\hat{\mathbf{s}}[n] = \begin{bmatrix} \hat{g}_L v[n] \\ \hat{g}_R v[n - \hat{d}_R] \end{bmatrix}. \quad (\text{B.7})$$

Since all spatial error are theoretically accountable by (1),  $\tilde{\mathbf{s}} \equiv \hat{\mathbf{s}}$ . The reference signal is given by

$$\mathbf{s}[n] = \begin{bmatrix} g_L \\ g_R \end{bmatrix} \cdot v[n], \quad (\text{B.8})$$

and  $E_{\mathbf{s}} = \sum_n \|\mathbf{s}[n]\|^2 = E_v$  since  $g_L^2 + g_R^2 = 1$ .

#### A. Panning Error

Where only panning error is present,  $\hat{d}_R = 0$ . Therefore,

$$u = \left( \sum_n \|\tilde{\mathbf{s}}[n] - \mathbf{s}[n]\|^2 \right)^{-1} \left( \sum_n \|\mathbf{s}[n]\|^2 \right) \quad (\text{B.9})$$

$$u^{-1} E_v = \sum_n \left\| \begin{bmatrix} \hat{g}_L - g_L \\ \hat{g}_R - g_R \end{bmatrix} \cdot v[n] \right\|^2 \quad (\text{B.10})$$

$$= [(\hat{g}_L - g_L)^2 + (\hat{g}_R - g_R)^2] \cdot E_v \quad (\text{B.11})$$

$$u^{-1} = 2 - 2 \cos \left( \frac{\pi}{4} (\hat{p} - p) \right). \quad (\text{B.12})$$

#### B. Panning and Delay Error

With  $\hat{d}_R \neq 0$ ,

$$u^{-1} E_v = \sum_n \left\| \begin{bmatrix} (\hat{g}_L - g_L)v[n] \\ \hat{g}_R v[n - \hat{d}_R] - g_R v[n] \end{bmatrix} \right\|^2 \quad (\text{B.13})$$

$$= (\hat{g}_L - g_L)^2 E_v + \sum_n \left| \hat{g}_R v[n - \hat{d}_R] - g_R v[n] \right|^2 \quad (\text{B.14})$$

$$u^{-1} = (\hat{g}_L - g_L)^2 + (\hat{g}_R - g_R)^2 + \frac{2\hat{g}_R g_R}{E_v} \left[ 1 - \sum_n v[n - \hat{d}_R]v[n] \right] \quad (\text{B.15})$$

$$u^{-1} = 2 - 2 \cos \left( \frac{\pi}{4} (\hat{p} - p) \right) + 2\hat{g}_R g_R \left( 1 - \frac{\kappa_v[-\hat{d}_R]}{\kappa_v[0]} \right), \quad (\text{B.16})$$

where  $\kappa_v[\cdot]$  is the autocorrelation function of  $v$ . Since  $|\kappa_v[d]| \leq \kappa_v[0]$  for all  $d$ , we have

$$0 \leq u^{-1} - 2 - 2 \cos \left( \frac{\pi}{4} (\hat{p} - p) \right) \leq 4\hat{g}_R g_R. \quad (\text{B.17})$$

### C. ADDITIONAL EXPERIMENTAL RESULTS

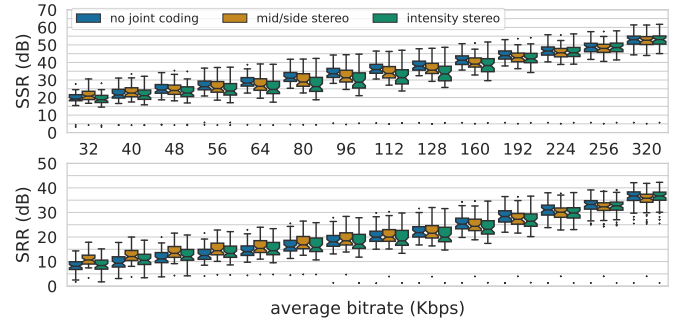


Fig. A1. SSR and SRR of the test signals compressed by AAC, by operating mode and average bitrates.

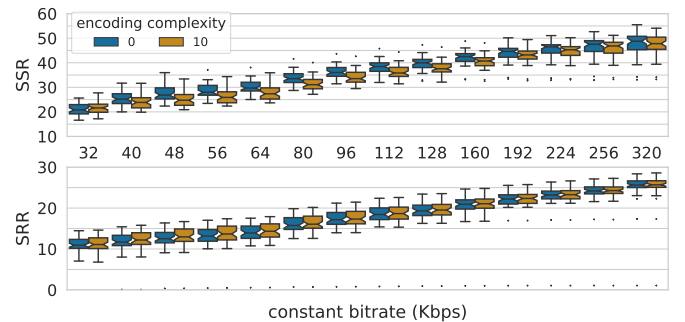


Fig. A2. SSR and SRR of the test signals compressed by Opus, by operating mode and constant bitrates.